Journal of Energy Chemistry 38 (2019) 8–14

Contents lists available at ScienceDirect

Journal of Energy Chemistry

journal homepage: www.elsevier.com/locate/jechem

http://www.journals.elsevier.com/journal-of-energy-chemistry/

Core-branch CoNi hydroxysulfides with versatilely regulated electronic and surface structures for superior oxygen evolution electrocatalysis

Bin Wang[a,b,1], Cheng Tang[a,c,1], Hao-Fan Wang[a,d], Xiao Chen[a], Rui Cao[b], Qiang Zhang[a,*]

[a] Beijing Key Laboratory of Green Chemical Reaction Engineering and Technology, Department of Chemical Engineering, Tsinghua University, Beijing 100084, China
[b] School of Chemistry and Chemical Engineering, Shaanxi Normal University, Xi'an 710119, Shaanxi, China
[c] School of Chemical Engineering, The University of Adelaide, Adelaide, Australia
[d] AIST-Kyoto University Chemical Energy Materials Open Innovation Laboratory (ChEM-OIL), National Institute of Advanced Industrial Science and Technology (AIST), Yoshida, Sakyo-ku, Kyoto 606-8501, Japan

ARTICLE INFO

Article history:
Received 17 November 2018
Revised 12 December 2018
Accepted 14 December 2018
Available online 28 December 2018

Keywords:
Oxygen evolution reaction
Hydroxysulfides
Anion regulation
Interfacial reaction
Hierarchical structure

ABSTRACT

To satisfy the rapid development of gas-involving electrocatalysis (O_2, CO_2, N_2, etc.), nanostructured electrocatalysts with favorably regulated electronic structure and surface nanostructures are urgently required. Herein, we highlighted a core-branch hydroxysulfide as a significantly enhanced oxygen evolution reaction electrocatalyst. This hydroxysulfide was facilely fabricated via a versatile interfacial reaction in S^{2-} inorganic solution at room temperature for a designed period. The moderative growth kinetics contributed to the growth of interconnected hydroxysulfide nanosheets with high-sulfur contents on the hydroxide precursor substrates, resulting in a hierarchical nanostructure with multifunctional modifications, including regulated electronic structure, rapid electron highway, excellent accessibility, and facilitated mass transfer. Such synthetic methodology can be generalized and facilely governed by regulating the temperature, concentration, duration, and solvent for targeted nanostructures. Contributed to the favorably regulated electronic structure and surface nanostructure, the as-obtained core-branch $Co_2NiS_{2.4}(OH)_{1.2}$ sample exhibits superior OER performance, with a remarkably low overpotential (279 mV required for 10.0 mA cm^{-2}), a low Tafel slope (52 mV dec^{-1}), and a favorable long-term stability. This work not only presents a promising nanostructured hydroxysulfide for excellent OER electrocatalysis, but also shed fresh lights on the further rational development of efficient electrocatalysts.

1. Introduction

Nanostructured electrocatalysts with effective active sites and favorable local environments are urgently required in view of the rapid development of gas-involving electrocatalysis (O_2, CO_2, N_2, etc.) [1,2]. On one hand, the active sites are responsible for the adsorption of reactants, bond breaking and forming, interfacial charge transfer, and desorption of products, which can be optimized by the regulation of electronic structures via heteroatom doping [3], defects [4], anion and cation modulation [5], etc. On the other hand, the local environment can also play critical roles on the electrocatalytic process [1,6] by affecting the active site accessibility, mass diffusion, concentration gradient, and electrochemical double-layer, which can be governed by the surface nanostructure or chemical modification [7,8]. Oxygen evolution reaction (OER), one of the most representative and crucial gas-involving electrocatalysis, is coupled with various renewable energy systems and significant for the future energy scenario [9]. It involves a multistep electron transfer process ($4OH^- \rightarrow 2H_2O + O_2 + 4e^-$) and thus considerably suffers from sluggish kinetics [10]. To date, although precious metal oxides (such as IrO_2 and RuO_2) have demonstrated excellent OER activities [11], their low abundance, high cost, and poor durability prohibit the practical applications. Instead, various transition-metal-based catalysts (such as oxides [12,13], chalcogenides [14,15], nitrides [16], and phosphides [17]) have been proposed and demonstrated promising OER reactivity, emerging as a versatile family of alternatives.

Among them, the sulfur-containing compounds, such as sulfides [18,19] and hydroxysulfides [20–23], have recently drawn particular attention due to their superior activity, remarkable stability, economic viability, and tunable features [24]. Generally, a relatively high sulfur anion content is desired for sulfur-containing compounds with excellent intrinsic OER activity [25]. The

* Corresponding author.
E-mail address: zhang-qiang@mails.tsinghua.edu.cn (Q. Zhang).
[1] These authors contributed equally to this work.

https://doi.org/10.1016/j.jechem.2018.12.006

incorporation of sulfur can efficiently regulate the electronic structure through anion regulation [5]. Moreover, the dual-ligand synergistic modulation derived by S^{2-} and OH^- in hydroxysulfides renders a further optimized binding energies between metal and anion ligands, thereby resulting in significantly enhanced OER performance [22,26]. Besides, by introducing sulfur anions into transition-metal compounds with favorable architecture, both high intrinsic activity and favorable extrinsic physicochemical characters can be simultaneously achieved, such as CoS_x cube [26], NiS frame [27], Co_9S_8@MoS_2 core-shell structure [28], $Fe_{11.8\%}$-Ni_3S_2 particle film [29], $CuCo_2S_4$ sheets [30]. Nevertheless, a high-content sulfur always results in an undesired aggregation of sulfurized clusters [31], which is mainly attributed to the adoption of less mild fabrication conditions for a desired composition [32,33], and/or inherent limitations of employed synthetic methods [34]. It significantly hinders the design and development of advanced nanostructured materials for optimal energy electrocatalysis. Therefore, the smart material design and versatile synthetic strategy are urgently required for the controllable construction of advanced sulfur-containing compounds, aiming at comprehensively optimizing both the electronic structures for active sites and the surface nanostructure for local environment.

Herein, we proposed an emerging core-branch hydroxysulfide with fully-exposed high-sulfur transition-metal compounds and highly-opened porous surface, which can be facilely fabricated by a moderative interfacial growth methodology. The core-branch structure is confirmed by the detailed structural and composition characterizations at both bulk and surface regions. The sulfur-enriched surface provides abundant highly active sites with favorable electronic structure, while the interconnected porous scaffold ensures a beneficial local environment for mass transfer and triple-phase reactions. As a result, the constructed core-branch CoNi hydroxysulfide exhibits superior OER performance with remarkably low overpotential (279 mV required for 10.0 mA cm^{-2}), low Tafel slope (52 mV dec^{-1}), and favorable long-term stability. The structure-property relationship is carefully elucidated and the synthetic methodology is also investigated.

2. Experimental

2.1. Synthesis of hydroxide precursors

The $Co_{1.8}Ni(OH)_{5.6}$ hydroxide substrate was prepared by a homogeneous precipitation method. Typically, $CoCl_2{\cdot}6H_2O$, $NiCl_2{\cdot}6H_2O$ and hexamethyleneteramine (HMT) were dissolved in 400 mL deionized water with concentrations of 4.0, 2.0 and 36.0 mM, respectively. Then, the as-obtained solution was heated at 95 °C for 10 h under Ar flow and magnetic stirring, during which a green precipitate was generated. After cooled to room temperature under Ar protection, the hydroxides were collected by subsequent filtrating, washing with ethanol and deionized water, and finally air-drying for 24 h. The $Co(OH)_2$ substrates was prepared with 6.0 mM $CoCl_2{\cdot}6H_2O$ and no $NiCl_2{\cdot}6H_2O$ in the synthetic system under otherwise identical conditions.

2.2. Synthesis of hydroxysulfides

The $Co_2NiS_{2.4}(OH)_{1.2}$, $Co_{2.1}NiS_3(OH)_{0.2}$, $Co_{1.9}NiS_{1.7}(OH)_{2.4}$, and $Co_{1.9}NiS_{0.4}(OH)_5$ hydroxysulfides were prepared by simply immersing $Co_{1.8}Ni(OH)_{5.6}$ in 2.0 M Na_2S solution at room temperature for 120, 170, 24, and 15 h, respectively, with subsequent filtrating, washing with ethanol and deionized water and air-drying for 24 h. The solid-to-liquid mass ratio in the immersing system is 1: 40. $Co_2S_{0.9}(OH)_{2.2}$ was synthesized with a 120 h immersing duration and $Co(OH)_2$ as substrate under otherwise identical conditions. The $Co_{1.9}NiS_{2.6}(OH)_{0.6}$–HT hydroxysulfide was prepared through immersing $Co_{1.8}Ni(OH)_{5.6}$ in 2.0 M Na_2S for 15 h at 100 °C. Such sample was finally achieved after subsequent filtrating, washing with ethanol and deionized water, and air-drying for 24 h. A brief summary of synthetic conditions for all the samples was also presented in Table S1. All the samples were synthesized under an ambient atmosphere. The material formulas are obtained from the XPS data, with biding energy determining the valence states of species and considering composition and electric neutrality. Taking $Co_2NiS_{2.4}(OH)_{1.2}$ as example, both Co and Ni cations are revealed to be +2 valence state and S anions are −2 (Fig. 4(a) and (b)). Then considering the composition and electric neutrality, the formula is recogonized as $Co_2NiS_{2.4}(OH)_{1.2}$.

2.3. Characterization

A spherical aberration corrected transmission electron microscope (TEM) instrument (FEI Tecnai G2 F20) operated at 300 kV, a JEM 2010 (JEOL Ltd., Tokyo, Japan) operated at 120.0 kV, and a scanning electron microscope (SEM, JEOL JSM-7401F) operated at 3.0 kV were used to probe the morphology and structure of samples. Aiming at limiting beam damage in high-voltage spherical aberration corrected TEM, the beam intensity is limited around 2.6×10^5 A m^{-2} and a short collection duration of about 3 min was also employed when energy disperse spectrometer (EDS) measuring. Under these conditions, the spatial resolution is less than 0.08 nm. Crystal phases were investigated by X-ray diffraction patterns recorded on a Bruker D8 Advance diffractometer at 40.0 kV and 120 mA with Cu-K_α radiation. X-ray photoelectron spectroscopy (XPS) was measured by ESCALAB 250xi, with monochromatic Al $K\alpha$ as the excitation source.

2.4. Electrocatalytic performance evaluation

A three-electrode electrochemistry workstation (CHI 760D, CHI instrument, USA) was used for electrocatalytic measurements, with a platinum sheet and saturated calomel electrode (SCE) as counter and reference electrode, respectively. A rotating disk (RDE, Pine Research Instrument, USA) is used as working electrode with an areal loading of 0.25 mg cm^{-2} at 1600 rpm. The electrolyte is 0.10 M KOH and all the tests were carried out at 25 °C. Linear sweep voltammetry (LSV) was recorded with 95% iR-compensation at 5.0 mV s^{-1}. The equation $\eta = E_{\text{versus SCE}} + 0.592\,\text{pH} + 0.241 - 1.23$ was used to calculate the overpotential (η). Tafel slope was calculated through the equation $\eta = b\log(j/j_0)$, where η is the overpotential, b is the Tafel slope, j and j_0 represent the current density and exchange current density, respectively. A set of scan-rate dependent capacitance currents were measured to determine the electrochemically active surface area (ECSA) through cyclic voltammetry (CV). The potential window versus reversible hydrogen electrode (RHE) is 1.00–1.05 V and the scan rates ranged from 10 to 100 mV s^{-1}. Electrochemical impedance spectroscopy (EIS) was measured at an OER potential of 1.78 V vs. RHE, with a frequency range of 10^{-1}–10^5 Hz and an amplitude of 5.0 mV.

3. Results and discussion

The core-branch CoNi hydroxysulfides ($Co_2NiS_{2.4}(OH)_{1.2}$) were fabricated via the controllable interfacial growth, as illustrated in Fig. 1(a). First, CoNi hydroxides ($Co_{1.8}Ni(OH)_{5.6}$) were synthesized as precursors and substrates in advance. Their nucleation and growth was decelerated and prolonged by the protection of inert gas from oxidation and CO_3^{2-} intercalation [35], thereby resulting in a hexagonal plate-like morphology (Fig. S1). Then the as-obtained CoNi hydroxides were immersed in a 2.0 M Na_2S aqueous solution for 120 h under room temperature, during which the surface layer was sufficiently converted into hydroxysulfides, owing

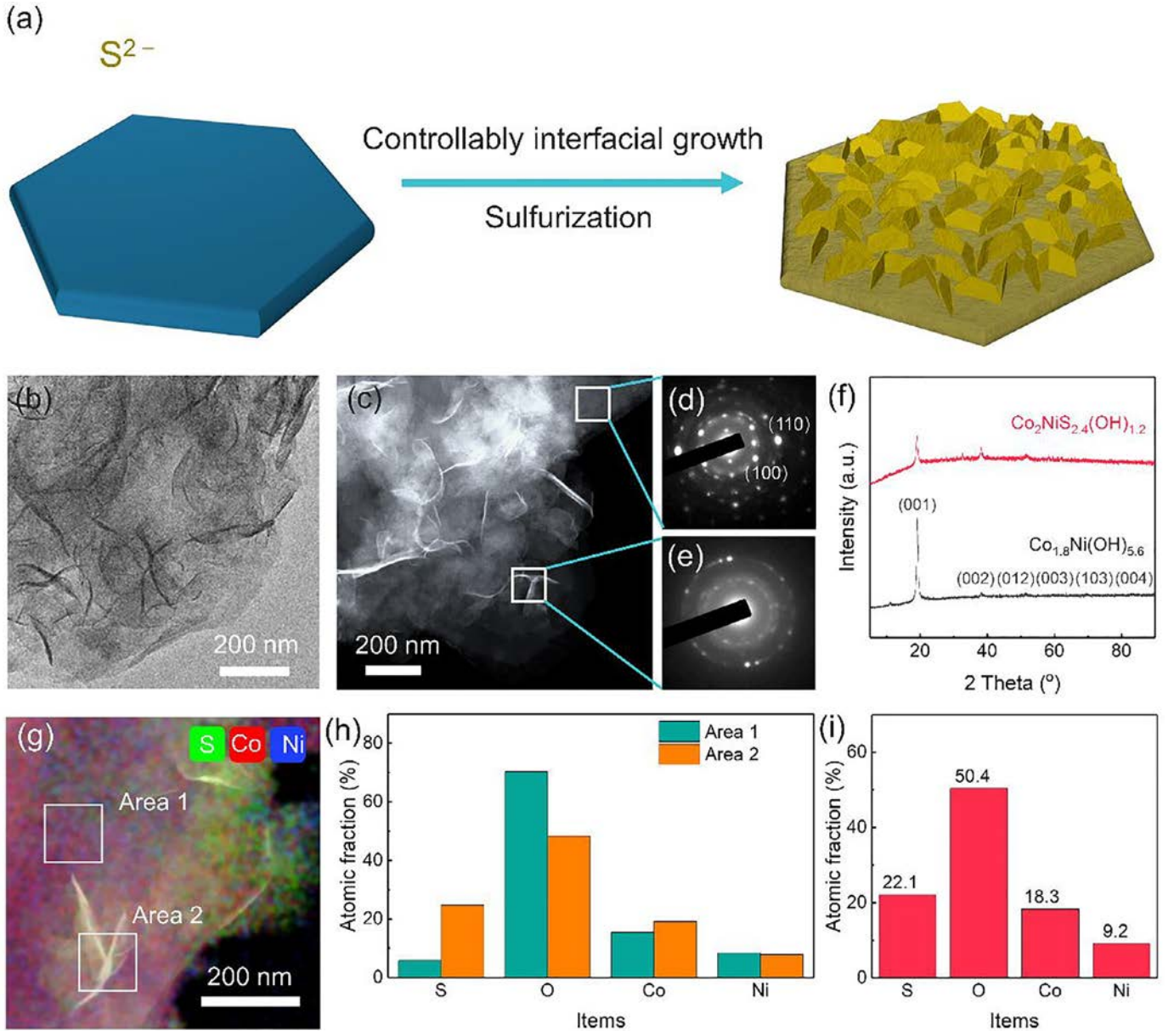

Fig. 1. Synthesis and characterizations of $Co_2NiS_{2.4}(OH)_{1.2}$ hydroxysulfide. (a) Schematic illustration of the fabrication of $Co_2NiS_{2.4}(OH)_{1.2}$, (b) TEM image, (c) HAADF-STEM image and (d) and (e) corresponding SAED patterns of different areas, (f) XRD patterns of $Co_2NiS_{2.4}(OH)_{1.2}$ and $Co_{1.8}Ni(OH)_{5.6}$, (g) HAADF-STEM image and corresponding EDS mapping, (h) elemental compositions in different areas measured by EDS, (i) elemental compositions detected by XPS.

to their markedly distinct solubilities (K_{sp}) [21]. For the elucidation of structure-property relationships, two control samples were prepared with an immersing duration of 24 h ($Co_{1.9}NiS_{1.7}(OH)_{2.4}$) and 170 h ($Co_{2.1}NiS_3(OH)_{0.2}$), respectively, under otherwise identical conditions (Table S1). Besides, a monometallic counterpart ($Co_2S_{0.9}(OH)_{2.2}$) was also synthesized when using $Co(OH)_2$ instead as the precursor (see details in Supporting Information).

The hierarchical morphology and chemical composition of as-fabricated hydroxysulfides were systematically characterized by transmission electron microscope (TEM), X-ray diffraction (XRD), energy-dispersive X-ray spectrometry (EDS), and X-ray photoelectron spectroscopy (XPS). As shown in Fig. 1(b), plenty of crinkled hydroxysulfide nanosheets are interconnected and assembled into a large plate-like structure for $Co_2NiS_{2.4}(OH)_{1.2}$, which is apparently different from the $Co_{1.8}Ni(OH)_{5.6}$ precursor (Fig. S1). The hydroxysulfide nanosheets are supposed to be generated from the surface of the hydroxide substrate during the interfacial reaction, while the bulk serves as a core matrix for the self-assembly of such a hierarchical structure. The in-situ generated hydroxysulfide nanosheets are ultrathin with a thickness dominantly less than 3 nm, benefiting the sufficient exposure of active sites (Fig. S2). When conducting the selected area electron diffraction (SAED) analysis at different regions in the $Co_2NiS_{2.4}(OH)_{1.2}$ sample (Fig. 1(c)), sets of relatively clear hexagonal spots can be observed in the bulk part (Fig. 1(d)), while basically broad rings with few clear spots are obtained in the surface part (Fig. 1(e)), indicating slightly different crystallinities. A set of brucite-like characteristic peaks (JCPDS No. 89-8616) can be observed in the XRD spectra (Fig. 1(f)), representing a *R*3*m* symmetry and hexagonal lattice for both $Co_2NiS_{2.4}(OH)_{1.2}$ and $Co_{1.8}Ni(OH)_{5.6}$. The peak intensities for $Co_2NiS_{2.4}(OH)_{1.2}$ are evidently lower than those for $Co_{1.8}Ni(OH)_{5.6}$ precursor, which can be ascribed to the lower crystalline or lattice mismatch in the surface nanosheets [36], in consistent with the SAED results [35,37] and high-resolution TEM image (Fig. S3).

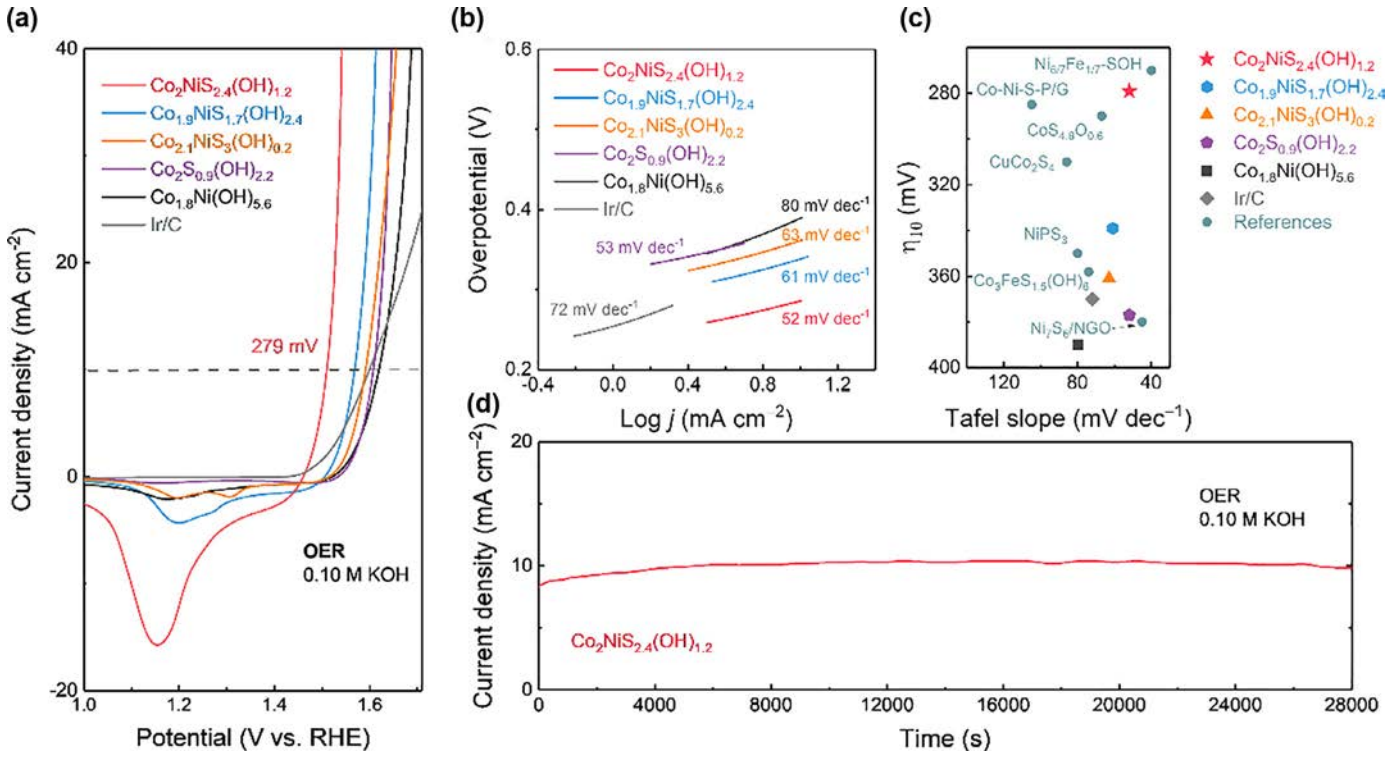

Fig. 2. OER performances of $Co_2NiS_{2.4}(OH)_{1.2}$ and control samples measured at 25 °C. (a) LSV curves obtained at a scan rate of 5.0 mV s^{-1} (the horizontal axis represents the potential versus reversible hydrogen electrode (RHE)), (b) Tafel plots, (c) figure of merit with respects to both activity and kinetics, with references all measured in alkaline electrolyte with RDE as working electrodes, (d) chronoamperometric response at an overpotential of 275 mV.

Furthermore, it is notable that the EDS analysis (Fig. 1(g) and (h), Fig. S4) exhibits a remarkably higher sulfur content of 24.7 at% for the surface hydroxysulfide sheets (area 2 in Fig. 1(g)) than that for the core substrate (area 1 in Fig. 1(g), 5.8 at%), suggesting the different compositions between the core and branch parts. The surface sulfur content is also detected to be as high as 22.1 at% by XPS (Fig. 1(i)), which is among the high level of similar hydroxysulfides and even comparable to that of sulfide materials reported so far (Table S2) [18,20–23,25,26,38–40]. This phenomenon indicates that the interfacial growth is prominently more efficient than surface sulfurization in introducing high-content sulfur phase.

Moreover, the sulfur content can be facilely increased by simply regulating the synthetic conditions, such as the immersing duration and/or S^{2-} concentration. With a longer immersing duration of 170 h, the resultant $Co_{2.1}NiS_3(OH)_{0.2}$ presents a similar nanostructure but an increased sulfur content of as high as 47.4 at% than $Co_2NiS_{2.4}(OH)_{1.2}$ (Fig. S5). In contrast, $Co_{1.9}NiS_{1.7}(OH)_{2.4}$, the one with a much shorter sulfurization time, still exhibits a 2D plate-like morphology similar to the hexagonal hydroxide precursor, and a lower sulfur content of 14.1 at% (Fig. S6). Therefore, the above results reveal that the proposed interfacial growth strategy is versatile and moderate for the targeted fabrication of nanostructured catalysts with favorable chemical compositions and surface morphologies, which can also be expanded to other materials, such as monometal hydroxides (Fig. S7) and layered double hydroxides (Fig. S8). Both the local structural and composition characterizations confirm the successful fabrication of a highly-opened core-branch CoNi hydroxysulfide, which exhibits several advantageous features: (1) fully exposed and accessible active sites due to the porous surface branches, (2) self-assemblied hierarchical structure resisting the nanoscale aggregation, (3) high-content of sulfur beneficial for intrinsic activity. With the regulated electronic structure and favorable porous architecture, the as-fabricated core-branch $Co_2NiS_{2.4}(OH)_{1.2}$ is thus expected to be an attractive candidate for OER electrocatalysis.

The electrocatalytic performance of as-fabricated hydroxysulfides was investigated on a rotating disk electrode (RDE) with an areal loading of 0.25 mg cm^{-2} in 0.10 M KOH. To avoid the disturbance from the oxidation current of Ni^{2+} to Ni^{3+} and Co^{2+} to Co^{3+}, the linear sweep voltammetry (LSV) polarization curves were swept from the high to low potential [36]. As shown in Fig. 2(a), $Co_2NiS_{2.4}(OH)_{1.2}$, $Co_{1.9}NiS_{1.7}(OH)_{2.4}$, and $Co_{2.1}NiS_3(OH)_{0.2}$ all present lower onset potentials and larger current densities than the $Co_{1.8}Ni(OH)_{5.6}$ precursor, indicating an obviously improved OER electrocatalysis originated from the sulfur incorporation. Among these hydroxysulfide samples, the core-branch $Co_2NiS_{2.4}(OH)_{1.2}$ exhibits a higher reactivity than the plate-like $Co_{1.9}NiS_{1.7}(OH)_{2.4}$ with a lower sulfurization degree, as well as the $Co_{2.1}NiS_3(OH)_{0.2}$ sample with a similar nanostructure but higher sulfur content. It highlights the vital role of a moderately high sulfur content and fully exposed architecture in optimizing the electrocatalytic performance. Notably, evident peaks are arisen around 1.2 V (vs. RHE) in the LSV curves, which are attributed to the redox process of Ni^{3+} to Ni^{2+} and Co^{3+} to Co^{2+}. A larger peak area indicates a higher transformation degree of metal cations in pristine catalysts to higher valance state species, which possess superior OER activity to the low ones and are more favorable for the electrocatalytic process. $Co_2NiS_{2.4}(OH)_{1.2}$ presents a prominently higher redox peak than others, further verifying the benefit of controllable anion regulation and the unique nanostructure in OER electrocatalysis through the controllable sulfurization in this work. In addition, the OER activity of $Co_2NiS_{2.4}(OH)_{1.2}$ is also significantly superior to that of $Co_2S_{0.9}(OH)_{2.2}$, which can be attributed to the partial-charge-transfer effect [33,41], revealing the preference of mixed metals rather than a highly stable monometallic material towards fully enhanced activities.

Tafel slope is employed to probe the OER kinetics [42]. As shown in Fig. 2(b), $Co_2NiS_{2.4}(OH)_{1.2}$ delivers a Tafel slop as low as 52 mV dec^{-1}. It is much lower than those of $Co_{1.9}NiS_{1.7}(OH)_{2.4}$ (61 mV dec^{-1}), $Co_{2.1}NiS_3(OH)_{0.2}$ (63 mV dec^{-1}),

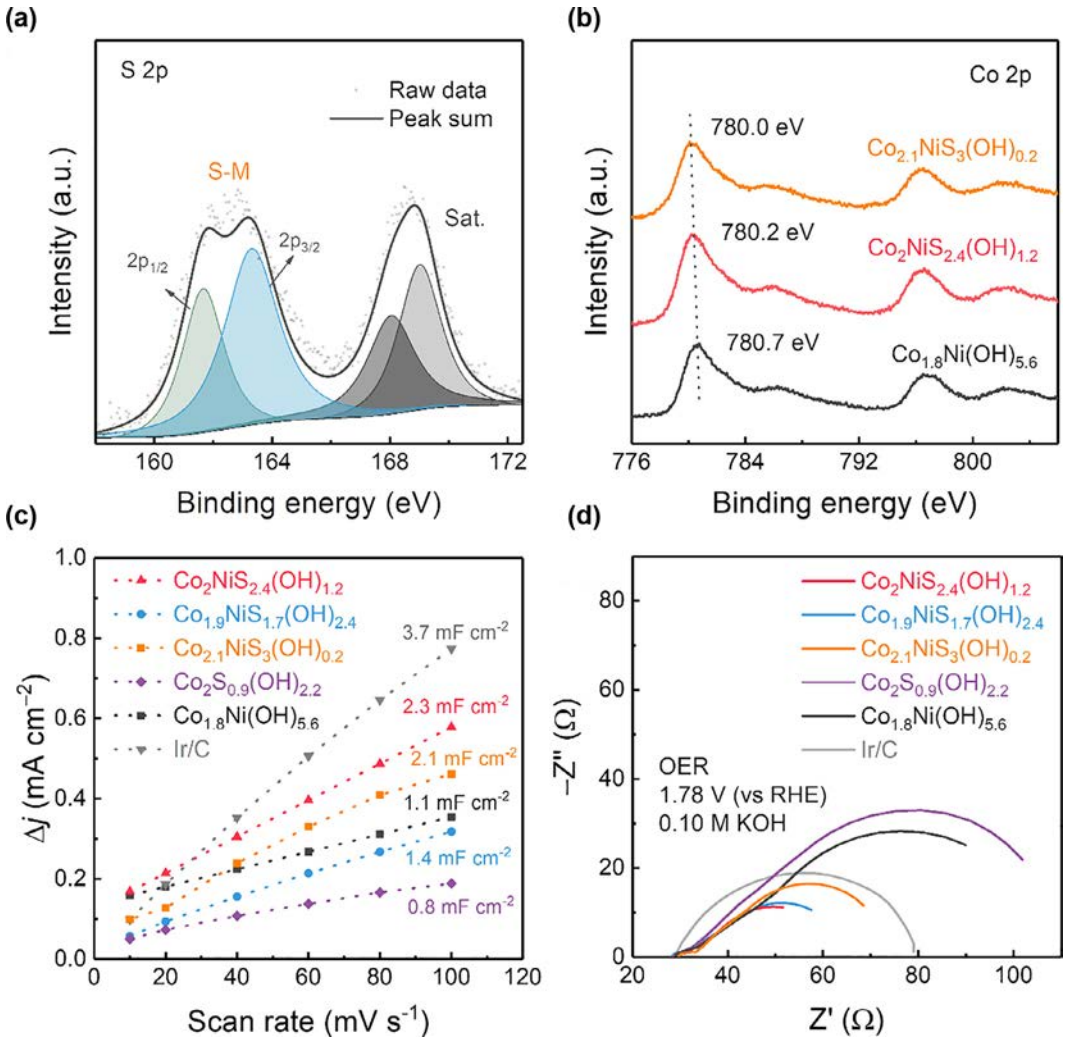

Fig. 3. Enhanced OER performances attributed to the regulated electronic and surface structures. (a) High-resolution S 2*p* and (b) high-resolution Co 2*p* XPS spectra of $Co_2NiS_{2.4}(OH)_{1.2}$ and control samples, (c) ECSA estimation based on charging current density differences plotted against scan rates, (d) Nyquist plots obtained from EIS measurements.

$Co_2S_{0.9}(OH)_{2.2}$ (53 mV dec^{-1}), and $Co_{1.8}Ni(OH)_{5.6}$ (80 mV dec^{-1}), indicating accelerated kinetics for the constructed hydroxysulfides. As a result, $Co_2NiS_{2.4}(OH)_{1.2}$ delivers a considerably higher current density at the same driven overpotential (η), obtaining a current density of 40.0 mA cm^{-2} at $\eta \approx 310$ mV, which is around ten-fold the current densities of the $Co_{1.8}Ni(OH)_{5.6}$ precursor and commercial Ir/C catalysts. The distinct activities and kinetics also suggest a changed active species and rate limiting step for $Co_2NiS_{2.4}(OH)_{1.2}$ [43]. Taking the overpotential required for 10 mA cm^{-2} (η_{10}), corresponding to 10% efficient solar water-splitting [44], and Tafel slop as OER performance evaluation merits, $Co_2NiS_{2.4}(OH)_{1.2}$ is comprehensively compared with similar catalysts from this work and references, with the regard to both activity and kinetics. As shown in Fig. 2(c), $Co_2NiS_{2.4}(OH)_{1.2}$ is demonstrated as an outstanding OER electrocatalyst, which is greatly superior to other hydroxsulfide and hydroxide samples, and even the precious Ir/C catalyst, and also among the best results of similar sulfur-containing metal materials reported so far (Table S3) [21,26,30,45–48].

Noteworthily, nanostructured electrocatalysts widely undergo potential-induced property transformations during OER process, including nanostructure, compositions, oxidation states and even local/surface phases, which is more evident in the case of sulfur containing compounds [45,49]. Accordingly, the long-term stability of $Co_2NiS_{2.4}(OH)_{1.2}$ and the characters of the sample after electrocatalysis are further investigated. As shown in Fig. S9, the 3D nanostructure with hierarchical porous surface of $Co_2NiS_{2.4}(OH)_{1.2}$ is well preserved after long-term OER, indicating a good structural stability. However, the surface sulfur content determined by XPS is obviously decreased from 22.1 to 13.8 at%, while the oxygen content is increased from 50.4 to 51.6 at%. It indicates a mild reorganization of $Co_2NiS_{2.4}(OH)_{1.2}$ surface by oxygen replacement, which mainly occurs on the surface within several nanometer depth, as revealed by the negatively correlated O and S contents near the plate edge (Fig. S9(e) and (f)). It should be noted that such surface reorganization is actually difficult to avoid in heterogeneous electrocatalysis under a positive bias; nevertheless, it is not necessarily a bad thing. The reorganized surface is expected to be more stable during operation conditions, and even further optimized active sites [50], which is evidenced by the favorable long-term durability at 10 mA cm^{-2} with an initial activation period (Fig. 2(d)).

These results indicate that remarkably enhanced OER performance with superior activity, rapid kinetics, and favorable durability can be obtained for the novel core-branch CoNi hydroxysulfide with both electronic structure and surface nanostructure regulation. In the high-resolution S 2*p* XPS profile (Fig. 3(a)), the interaction between sulfur and metal ions can be revealed for $Co_2NiS_{2.4}(OH)_{1.2}$ [28,51]. Ascribing to higher polarizability of

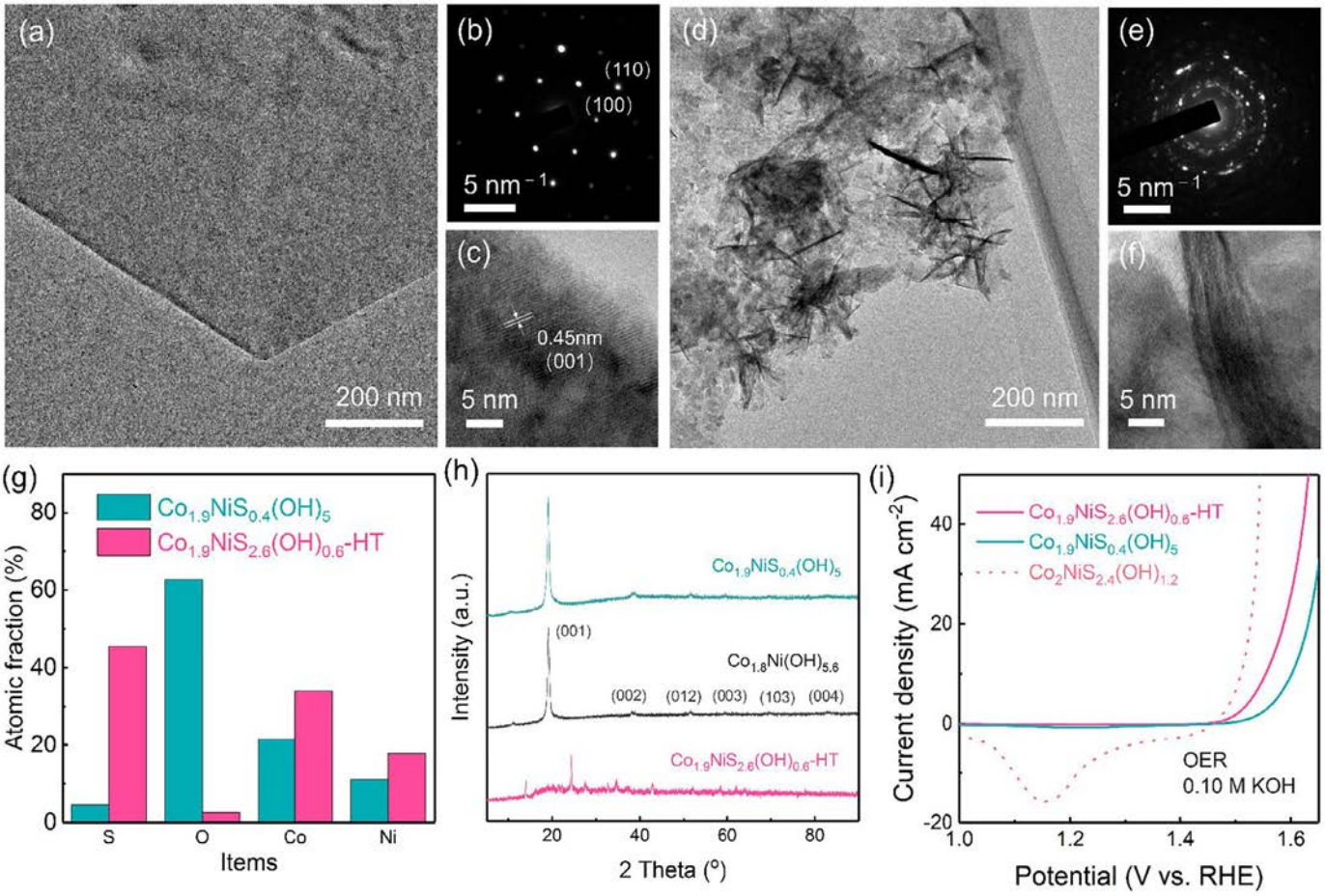

Fig. 4. The vital role of controllable interfacial growth in the construction of core-branch hydroxysulfide. (a) TEM image, (b) SAED pattern, and (c) HRTEM image of $Co_{1.9}NiS_{0.4}(OH)_5$. (d) TEM image, (e) SAED pattern, and (f) HRTEM image of $Co_{1.9}NiS_{2.6}(OH)_{0.6}$–HT. (g) Elemental compositions detected by XPS. (h) XRD patterns. (i) LSV curves obtained at a scan rate of 5.0 mV s^{-1}.

sulfur than pristine oxygen in hydroxide matrix, the incorporation of sulfur into lattices is reported to disperse more electrons to the 3*d* orbits of cationic active sites, leading to a regulation to the electronic structure. Notably, an insufficient incorporation of sulfur affords a too strong positive electric field, which is not facilitated for efficient oxygen desorption. In contrast, an excessive introduction results in a weak one, unfavorable for hydroxyl adsorption adversely [25]. The high-resolution Co 2*p* profiles exhibit a moderate biding energy shift of $Co_2NiS_{2.4}(OH)_{1.2}$ than that of $Co_{2.1}NiS_3(OH)_{0.2}$ compared to $Co_{1.8}Ni(OH)_{5.6}$ precursors (Fig. 3(b)). It indicates a controllable anion regulation in electronic structure for $Co_2NiS_{2.4}(OH)_{1.2}$, rendering a more balanced electric field for intermediate chemisorption and thus improved electrocatalytic activities via anion regulation [20,21]. As a result, $Co_2NiS_{2.4}(OH)_{1.2}$ exhibits higher OER reactivity than hydroxide precursors and other hydroxysulfide samples. Besides, more CoNi species in $Co_2NiS_{2.4}(OH)_{1.2}$ are converted into high-valence cations during OER, suggested by the larger redox peak in LSV curves (Figs. 2(a) and S10) [52]. The high-valence metal species, like CoOOH and NiOOH, are believed to be crucial and beneficial to the higher OER reactivities [53,54]. In addition, the impressive nanostructure also significantly contributes to the improved OER performance. As shown in Fig. 3(c), a prominently higher electrochemically active surface area (ECSA) estimated by double-layer capacitance (C_{dl}) is obtained by $Co_2NiS_{2.4}(OH)_{1.2}$ compared with other samples, suggesting a fully exposed nanostructure and considerably more accessible active sites for electrocatalysis. The 3D interconnected hydroxysulfide framework and the delocalization of metal d electrons derived from the sulfur introduction can lead to an electron and charge highway [55], as revealed by a lower electrochemically resistance of $Co_2NiS_{2.4}(OH)_{1.2}$ (Fig. 3(d)). Furthermore, the hierarchical porous architecture of core-branch hydroxysulfides, constructed by the interconnected macropores and meso/micro pores over the whole scaffolds, provides a more favorable local environment compared with the pristine hydroxide flakes, with abundant free channels for mass transfer, facilitated ion insertion/extraction and gas diffusion, which is significant for gas-involved triple-phase OER process.

To further probe the growth behavior and activity mechanism for such interfacial engineered nanomaterials, two control samples fabricated in high temperature ($Co_{1.9}NiS_{2.6}(OH)_{0.6}$–HT) and room temperature ($Co_{1.9}NiS_{0.4}(OH)_5$), respectively, using the same short immersing duration (15 h), were further employed. With a short reaction duration and slow growth kinetics, $Co_{1.9}NiS_{0.4}(OH)_5$ also presents a plate-like morphology and a low sulfur content (4.6 at%) similar to $Co_{1.9}NiS_{1.7}(OH)_{2.4}$ (Fig. 4(a) and (g)). However, a set of clear hexagonally arranged spots is shown in the SAED pattern (Fig. 4(b)), which is the same as that for the hydroxide precursor (Fig. S1(c)). It reveals a hydroxide bulk and only a slight sulfurization for $Co_{1.9}NiS_{0.4}(OH)_5$ due to the insufficient interfacial reaction, which can also be manifested by the lattice fringes shown in Fig. 4(c). In spite of the short immersing duration, the $Co_{1.9}NiS_{2.6}(OH)_{0.6}$–HT can also exhibit a 3D architecture with interconnected nanosheets (Fig. 4(d)), which can be rationalized by an expected acceleration in interfacial growth at a higher temperature. Nevertheless, the core-branch structure cannot be obtained

without new crystalline phases generated (Fig. 4(e) and (h)), and obvious stacking of the hydroxysulfide sheets and aggregation of sulfurized clusters (Figs. 4f and S11). Besides, the sulfur content of $Co_{1.9}NiS_{2.6}(OH)_{0.6}$–HT is detected as high as 45.6 at%, with almost all original oxygen being replaced by sulfur (Fig. 4(g)). These results indicate that both temperature and immersing duration are influential to the resultant materials, by determining the reaction rate and transformation depth. Consequently, the $Co_{1.9}NiS_{0.4}(OH)_5$ with insufficient regulation in electronic and surface structures and the $Co_{1.9}NiS_{2.6}(OH)_{0.6}$–HT with overdeveloped structure and composition both deliver a considerably inferior OER performance to $Co_2NiS_{2.4}(OH)_{1.2}$ (Figs. 4(i) and S12).

4. Conclusions

An emerging core-branch CoNi hydroxysulfide has been rationally designed and facilely fabricated via a green and controllable interfacial reaction by simply immersing hydroxide precursors in S^{2-} inorganic solution at room temperature for a designed period. Crinkled and interconnected hydroxysulfide nanosheets with high-sulfur content are vertically grow on the precursor substrate, resulting in a hierarchical nanostructure with multifunctional modifications, including regulated electronic structure by anion regulation, electron highway in the interconnected hydroxysulfide scaffold, excellent accessibility, and facilitated mass transfer due to the highly opened core-branch structure and ultrathin nanosheets. The synthetic strategy can be expanded to other material system, and can be facilely controlled by changing the temperature, concentration, duration, and solvent for targeted nanostructures. Contributed to the regulated electronic structure and surface nanostructure, the $Co_2NiS_{2.4}(OH)_{1.2}$ sample exhibits superior OER performance, with a considerably decreased overpotential (279 mV required for 10.0 mA cm^{-2}), a remarkably low Tafel slope (52 mV dec^{-1}), and a favorable long-term stability. This work not only demonstrates a novel nanostructured hydroxysulfides for excellent OER electrocatalysis, but also provides a new concept of interfacial engineering and versatile synthetic methodology for the fabrication of advanced materials with both electronic structure and surface nanostructure regulation, which is instructive and promising in a various field of electrocatalysis, such as oxygen evolution, hydrogen evolution, carbon dioxide reduction, nitrogen reduction reactions.

Acknowledgments

This work was supported by the National Key Research and Development Program (2016YFA0202500 and 2016YFA0200101) and the Natural Scientific Foundation of China (21825501). We thank Bo-Quan Li, Xiao-Yang Cui, Xiao-Meng Liu, Nannan Sun, and Ling Zhong for helpful discussion.

Supplementary material

Supplementary material associated with this article can be found, in the online version, at doi:10.1016/j.jechem.2018.12.006.

References

[1] C. Tang, H.-F. Wang, Q. Zhang, Acc. Chem. Res. 51 (2018) 881–889.
[2] M. Dunwell, W. Luc, Y. Yan, F. Jiao, B. Xu, ACS Catal. 8 (2018) 8121–8129.
[3] K. Gong, F. Du, Z. Xia, M. Durstock, L. Dai, Science 323 (2009) 760–764.
[4] C. Tang, H.F. Wang, X. Chen, B.Q. Li, T.Z. Hou, B. Zhang, Q. Zhang, M.M. Titirici, F. Wei, Adv. Mater. 28 (2016) 6845–6851.
[5] H.-F. Wang, C. Tang, B.-Q. Li, Q. Zhang, Inorg. Chem. Front. 5 (2018) 521–534.
[6] Y.P. Zhu, C. Guo, Y. Zheng, S.-Z. Qiao, Acc. Chem. Res. 50 (2017) 915–923.
[7] M. Qiao, C. Tang, L.C. Tanase, C.M. Teodorescu, C. Chen, Q. Zhang, M.-M. Titirici, Mater. Horiz. 4 (2017) 895–899.
[8] Y. Zheng, Y. Jiao, S.Z. Qiao, Adv. Mater. 27 (2015) 5372–5378.
[9] J.A. Turner, Science 305 (2004) 972–974.
[10] Y. Zhang, X. Fan, J. Jian, D. Yu, Z. Zhang, L. Dai, Energy Environ. Sci. 10 (2017) 2312–2317.
[11] Y. Lee, J. Suntivich, K.J. May, E.E. Perry, Y. Shao-Horn, J. Phys. Chem. Lett. 3 (2012) 399–404.
[12] H. Osgood, S.V. Devaguptapu, H. Xu, J. Cho, G. Wu, Nano Today 11 (2016) 601–625.
[13] X. Zhao, W. Zhang, R. Cao, J. Energy Chem. 26 (2017) 1210–1216.
[14] S. Deng, S. Shen, Y. Zhong, K. Zhang, J. Wu, X. Wang, X. Xia, J. Tu, J. Energy Chem. 26 (2017) 1203–1209.
[15] H. Ren, Z.-H. Huang, Z. Yang, S. Tang, F. Kang, R. Lv, J. Energy Chem. 26 (2017) 1217–1222.
[16] S.L. Zhao, M. Li, M. Han, D.D. Xu, J. Yang, Y. Lin, N.E. Shi, Y.N. Lu, R. Yang, B.T. Liu, Z.H. Dai, J.C. Bao, Adv. Funct. Mater. 28 (2018) 1706018.
[17] Z. Zhou, N. Mahmood, Y. Zhang, L. Pan, L. Wang, X. Zhang, J.-J. Zou, J. Energy Chem. 26 (2017) 1223–1230.
[18] P. Ganesan, M. Prabu, J. Sanetuntikul, S. Shanmugam, ACS Catal. 5 (2015) 3625–3637.
[19] H. Yuan, L. Kong, T. Li, Q. Zhang, Chin. Chem. Lett. 28 (2017) 2180–2194.
[20] B. Wang, C. Tang, H.F. Wang, B.Q. Li, X. Cui, Q. Zhang, Small Methods (2018) 1800055.
[21] H.F. Wang, C. Tang, B. Wang, B.Q. Li, Q. Zhang, Adv. Mater. 29 (2017) 1702327.
[22] L. Peng, J. Wang, Y. Nie, K. Xiong, Y. Wang, L. Zhang, K. Chen, W. Ding, L. Li, Z. Wei, ACS Catal. 7 (2017) 8184–8191.
[23] K. Xiang, J. Guo, J. Xu, T. Qu, Y. Zhang, S. Chen, P. Hao, M. Li, M. Xie, X. Guo, ACS Appl. Energy Mater. 1 (2018) 4040–4049.
[24] L. Han, S. Dong, E. Wang, Adv. Mater. 28 (2016) 9266–9291.
[25] B.Q. Li, S.Y. Zhang, C. Tang, X. Cui, Q. Zhang, Small 13 (2017) 1700610.
[26] P. Cai, J. Huang, J. Chen, Z. Wen, Angew. Chem. Int. Ed. 56 (2017) 4858–4861.
[27] X.Y. Yu, L. Yu, H.B. Wu, X.W. Lou, Angew. Chem. Int. Ed. 54 (2015) 5331–5335.
[28] H. Zhu, J. Zhang, R. Yanzhang, M. Du, Q. Wang, G. Gao, J. Wu, G. Wu, M. Zhang, B. Liu, Adv. Mater. 27 (2015) 4752–4759.
[29] N. Cheng, Q. Liu, A.M. Asiri, W. Xing, X. Sun, J. Mater. Chem. A 3 (2015) 23207–23212.
[30] M. Chauhan, K.P. Reddy, C.S. Gopinath, S. Deka, ACS Catal. 7 (2017) 5871–5879.
[31] M.-R. Gao, Y.-F. Xu, J. Jiang, S.-H. Yu, Chem. Soc. Rev. 42 (2013) 2986–3017.
[32] L. Zeng, K. Sun, Z. Yang, S. Xie, Y. Chen, Z. Liu, Y. Liu, J. Zhao, Y. Liu, C. Liu, J. Mater. Chem. A 6 (2018) 4485–4493.
[33] X.Y. Yu, X.W. Lou, Adv. Energy Mater. 8 (2018) 1701592.
[34] Z. Peng, D. Jia, A.M. Al-Enizi, A.A. Elzatahry, G. Zheng, Adv. Energy Mater. 5 (2015) 1402031.
[35] J. Liang, R. Ma, N. Iyi, Y. Ebina, K. Takada, T. Sasaki, Chem. Mater. 22 (2009) 371–378.
[36] C. Hu, L. Zhang, Z.J. Zhao, A. Li, X. Chang, J. Gong, Adv. Mater. 30 (2018) 1705538.
[37] L. Zhang, W. Shi, B. Zhang, J. Energy Chem. 26 (2017) 1117–1135.
[38] Q. Liu, J. Jin, J. Zhang, ACS Appl. Mater. Interfaces 5 (2013) 5002–5008.
[39] M. Shen, C. Ruan, Y. Chen, C. Jiang, K. Ai, L. Lu, ACS Appl. Mater. Interfaces 7 (2015) 1207–1218.
[40] Y. Zeng, L. Chen, R. Chen, Y. Wang, C. Xie, T. Li, L. Huang, S. Wang, J. Mater. Chem. A 6 (2018) 24311–24316.
[41] C. Tang, H.-F. Wang, H.-S. Wang, F. Wei, Q. Zhang, J. Mater. Chem. A 4 (2016) 3210–3216.
[42] M.B. Stevens, L.J. Enman, A.S. Batchellor, M.R. Cosby, A.E. Vise, C.D. Trang, S.W. Boettcher, Chem. Mater. 29 (2016) 120–140.
[43] A. Holewinski, S. Linic, J. Electrochem. Soc. 159 (2012) 864–870.
[44] C.C. McCrory, S. Jung, J.C. Peters, T.F. Jaramillo, J. Am. Chem. Soc. 135 (2013) 16977–16987.
[45] B. Konkena, J. Masa, A.J. Botz, I. Sinev, W. Xia, J.r. Koßmann, R. Drautz, M. Muhler, W. Schuhmann, ACS Catal. 7 (2016) 229–237.
[46] T. Wang, G. Nam, Y. Jin, X. Wang, P. Ren, M.G. Kim, J. Liang, X. Wen, H. Jang, J. Han, Adv. Mater. 30 (2018) 1800757.
[47] H.J. Song, H. Yoon, B. Ju, G.H. Lee, D.W. Kim, Adv. Energy Mater. (2018) 1802319.
[48] D. Wang, Z.Y. Wang, Q.Q. Zhan, Y. Pu, J.X. Wang, N.R. Foster, L.M. Dai, Engineering 3 (2017) 402–408.
[49] C. Tang, M.-M. Titirici, Q. Zhang, J. Energy Chem. 26 (2017) 1077–1093.
[50] B.-Q. Li, Z.-J. Xia, B. Zhang, C. Tang, H.-F. Wang, Q. Zhang, Nat. Commun. 8 (2017) 934.
[51] L. Zhou, M. Shao, C. Zhang, J. Zhao, S. He, D. Rao, M. Wei, D.G. Evans, X. Duan, Adv. Mater. 29 (2017) 1604080.
[52] C. Tang, H.S. Wang, H.F. Wang, Q. Zhang, G.L. Tian, J.Q. Nie, F. Wei, Adv. Mater. 27 (2015) 4516–4522.
[53] M.W. Louie, A.T. Bell, J. Am. Chem. Soc. 135 (2013) 12329–12337.
[54] L. Zhou, M. Shao, M. Wei, X. Duan, J. Energy Chem. 26 (2017) 1094–1106.
[55] J. Yang, G. Zhu, Y. Liu, J. Xia, Z. Ji, X. Shen, S. Wu, Adv. Funct. Mater. 26 (2016) 4712–4721.